Journal of Applied Mathematics and Physics, 2022, 10, 3408-3423
https://www.scirp.org/journal/jamp
ISSN Online: 2327-4379
ISSN Print: 2327-4352

Extracting Multiple Nodes in a Brain Region of Interest for Brain Functional Network Estimation and Classification

Chengcheng Wang[1], Haimei Wang[1], Yifan Qiao[2], Yining Zhang[1*]

[1]School of Mathematics Science, Liaocheng University, Liaocheng, China
[2]International Center, Jinan Foreign Language School, Jinan, China
Email: *zhangyining@lcu.edu.cn

How to cite this paper: Wang, C.C., Wang, H.M., Qiao, Y.F. and Zhang, Y.N. (2022) Extracting Multiple Nodes in a Brain Region of Interest for Brain Functional Network Estimation and Classification. *Journal of Applied Mathematics and Physics*, **10**, 3408-3423.
https://doi.org/10.4236/jamp.2022.1011226

Received: October 17, 2022
Accepted: November 26, 2022
Published: November 29, 2022

Abstract

Purpose: Brain functional networks (BFNs) has become important approach for diagnosis of some neurological or psychological disorders. Before estimating BFN, obtaining blood oxygen level dependent (BOLD) representative signals from brain regions of interest (ROIs) is important. In the past decades, the common method is generally to take a ROI as a node, averaging all the voxel time series inside it to extract a representative signal. However, one node does not represent the entire information of this ROI, and averaging method often leads to signal cancellation and information loss. Inspired by this, we propose a novel model extraction method based on an assumption that a ROI can be represented by multiple nodes. **Methods:** In this paper, we first extract multiple nodes (the number is user-defined) from the ROI based on two traditional methods, including principal component analysis (PCA), and K-means (Clustering according to the spatial position of voxels). Then, canonical correlation analysis (CCA) was issued to construct BFNs by maximizing the correlation between the representative signals corresponding to the nodes in any two ROIs. Finally, to further verify the effectiveness of the proposed method, the estimated BFNs are applied to identify subjects with autism spectrum disorder (ASD) and mild cognitive impairment (MCI) from health controls (HCs). **Results:** Experimental results on two benchmark databases demonstrate that the proposed method outperforms the baseline method in the sense of classification performance. **Conclusions:** We propose a novel method for obtaining nodes of ROId based on the hypothesis that a ROI can be represented by multiple nodes, that is, to extract the node signals of ROIs with K-means or PCA. Then, CCA is used to construct BFNs.

Keywords

Brain Functional Network, Node Selection, Pearson's Correlation, Canonical

Correlation Analysis, Brain Disorder Classification

1. Introduction

The brain is a complex network with underlying organizational structures. In recent years, brain functional network (BFN) approach based on the correlation of spontaneous fluctuations in blood oxygen level dependent (BOLD) signals, has opened new insights into the function of the human brain [1]. BOLD-based brain functional network (BFN) constructed from functional magnetic resonance imaging (fMRI) data has been applied to understand the brain organizational patterns and diagnosis of neurological diseases [2] such as autism spectrum disorder (ASD) [3] [4] and mild cognitive impairment (MCI) [5] [6]. One of the critical questions is how to choose what the nodes represent for constructing a high-quality BFN. There is currently no universally accepted definition of nodes, which is also one of the most important issues in neuroimaging data network analysis.

Mathematically, the brain is depicted as a collection of nodes and edges/links. Specifically, each node corresponds to a brain region that should be functionally homogeneous in the brain, and each edge depicts a dependency between the BOLD signals associated with a pair of ROIs [7]. To date, researchers have developed many methods to select the brain network node. The first method is to treat single neurons as network nodes and synaptic connections as edges [8]. However, this microscopic approach is not suitable for studying the entire human brain, because the imaging method has insufficient resolution. The second option is voxel-wise method and the nodes are voxels (small cubes with edges of 2 - 8 mm) [9]. Currently, researchers have developed many several typical methods for voxel-wise estimation, including independent component analysis (ICA) [10], seed-based correlation analysis (SCA) [11], homogeneity (ReHo) [12], and fractional amplitude of low-frequency fluctuations (fALFF) [13]. Although the voxel-based BFN contains all the information of the whole brain, the calculation cost is too high because of the excessive number of voxels. On the other hand, voxel-based method lacks explanation like how strong is the functional connection between a pair of ROIs, thus it is hard to seek potential biomarkers to identify brain diseases. Finally, the third and most straightforward approach is to consider regions of interest (ROIs), using pre-defined clusters of anatomically close voxels, as nodes [14]. ROIs are usually defined using an anatomical atlas, based on structural MR images [14]. This approach is based on the assumption that voxels within ROIs are functionally similar, and each ROI contains 11-1512 voxels. The signals of ROIs are typically computed by averaging the BOLD signals of its voxels. Compared with voxel-level methods, this method not only significantly reduces the number of nodes, but also better explains the activity of connections between ROIs. Even though there are so many advantages to ROI-wise

method, it still has three drawbacks that deserve our attention:

1) One representative signal is not enough to represent all the information within a ROI and information may be lost after averaging the voxel signals within the anatomical region because ROIs defined based on natoical atlases are unlikely to reflect functional boundaries accurately (*i.e.*, a function may be distributed within several anatomical regions, or an anatomical region may contain multiple subareas with different functions [15]); 2) It is sensitive to potential noisy voxels in the ROI after averaging the BOLD signals over all voxels that make up the node; 3) Robustness may be reduced due to unclear definition of anatomical boundaries. Subtle changes in the position of voxels may alter the BOLD signals of ROIs after averaging, for example.

Despite the above widely-used methods, they also have their own drawbacks that cannot be ignored. To circumvent the difficulty of these problems, in this article, we propose a novel node define approach based on an assumption that a ROI can be represented by multiple nodes (the number n of nodes defined by user). Specifically, we choose two methods to extract nodes. The first is averaging method that K-means [16] is used to divide the voxels ROIs into uniform n groups according to their spatial position coordinates, and then average all the voxel signals in each group. And the second is principal component analysis (PCA) [17] which directly takes the eigenvectors corresponding to the first n largest eigenvalues as the fMRI time series corresponding to the selected n nodes. After extracting the time series signals of the nodes by the two methods mentioned above, we use CCA to construct BFNs. This is because typical correlation analysis (CCA), as a bivariate multivariate tool, can consider two datasets with different patterns simultaneously to reveal their underlying hidden associations [18]. For details, see **Figure 1**.

The main contributions of this work are as follows. First, we use two different methods to extract multiple representative time series for each ROI. Second, when calculating the correlation between a pair of ROIs, we use CCA to assign appropriate weights to the time series with different contributions for each ROI. In addition, our method not only allows more flexibility and discretion in determining the number of nodes in the ROI, but also saves computational cost.

In this article, the baseline approach we chose is to use ROIs as nodes, using simple and popular Pearson correlation (PC) [19] to estimate BFNs. To verify the effectiveness of the proposed method, the BFNs estimated by our method is validated on two datasets, that is, to identify the patients with ASD from health controls (HCs) on Autism Brain Imaging Data Exchange (ABIDE) dataset1 and to identify the patients with MCI from HCs on Alzheimer's Disease Neuroimaging Initiative (ADNI) dataset2. Experimental results demonstrate that the proposed model can significantly improve the classification performance compared with the baseline method.

The rest of this paper is organized as follows. In Section II, we first introduce the preprocessed data, review conventional BFN construction methods (*i.e.*, PC), and then develop our approach for BFN estimation. In Section III, we conduct

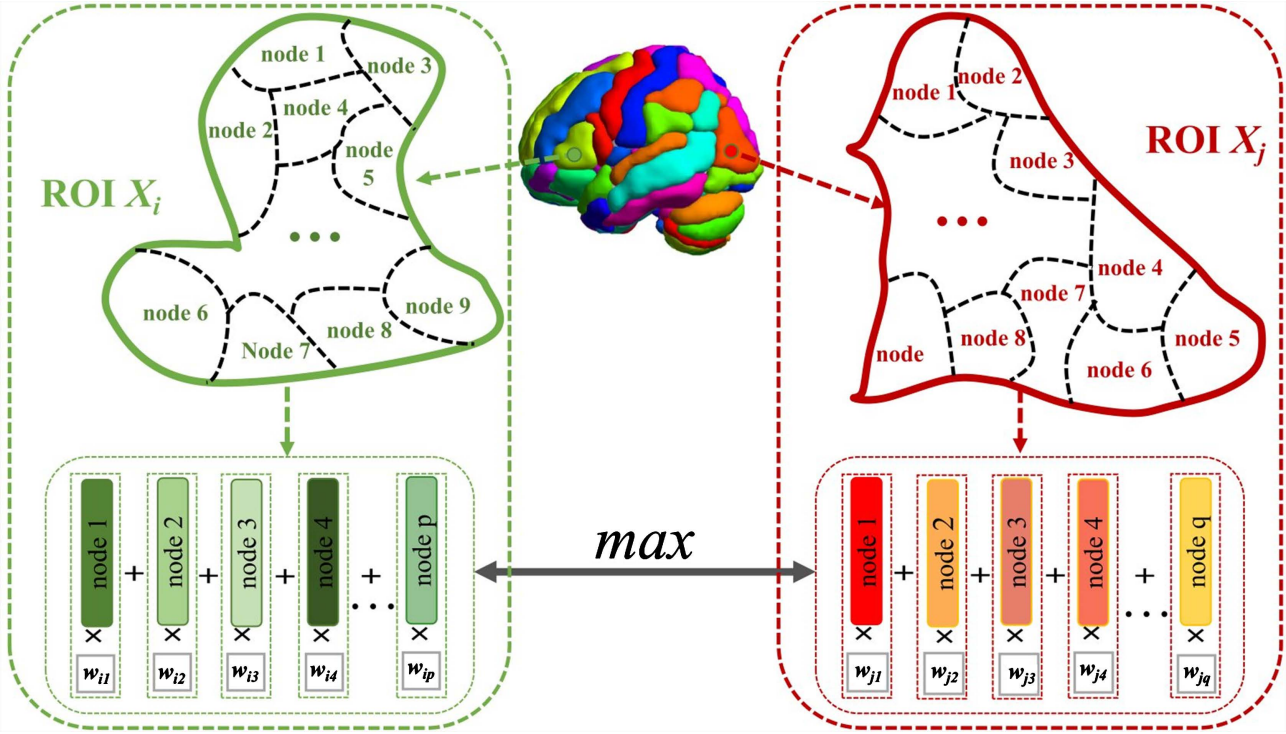

Figure 1. A general for constructing BFN by canonical correlation analysis. Where x_i and x_j represent BOLD time series of all voxels in *i*-th ROI and *j*-th ROI, and *p*, *q* are the number of nodes in the *i*-th and *j*-th ROIs respectively.

experiments for evaluating the proposed method by ASD/MCI identification. In Section IV, we discuss our findings and several aspects that affect the final performance. Besides, several limitations of this work as well as the possible research in the future directly. Finally, we briefly conclude this paper in Section V.

2. Materials and Methods

In this section, we describe data preparation (including data acquisition and preprocessing), the extracting node methods of ROIs and constructing BFN methods (including baseline and proposed methods). To better understand, we describe the pipeline of the entire classification task in Figure 2.

2.1. Data Preparation

In this section, we verify the validity of our proposed approach on two public datasets, i.e., ABIDE and ADNI databases. Demographic information of the subjects in ABIDE and ADNI databases is shown in Table 1.

ABIDE database: 184 subjects (including 79 ASDs and 105 HCs) are involved in our experiment for testing our proposed method. Concretely, the rs-fMRI data of the subjects are available in the largest site (*i.e.*, New York University (NYU)) of ABIDE database. Subjects from the dataset were scanned using a clinical routine 3.0T Tesla Allegra scanner with the following parameters: flip angle = 90˚, repetition time (TR)/echo time (TE) = 2000/15 ms, and voxel thickness = 4.0 mm. The scanning lasted 7 minutes, which generates 180 volumes for each subject.

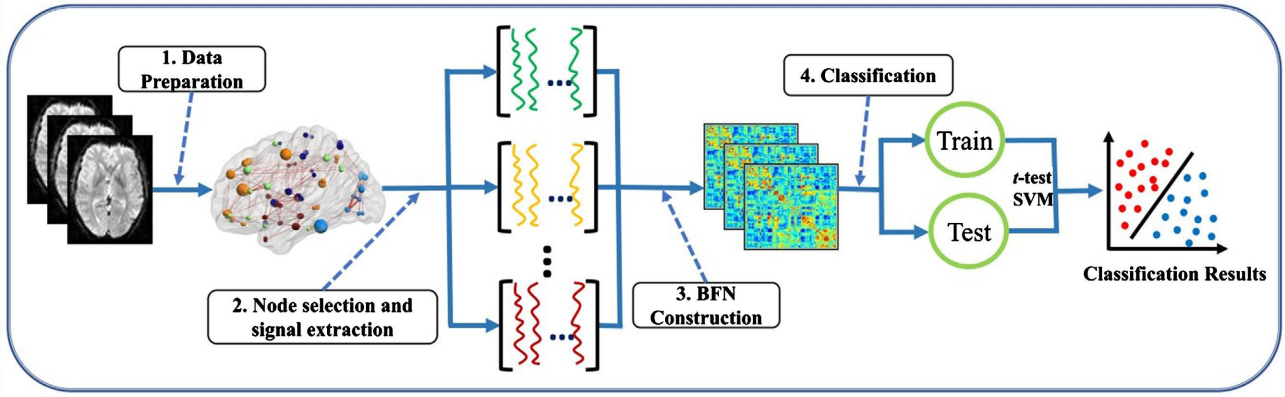

Figure 2. The main pipeline of disorder identification used in our study, which contains four major modules: 1) data preparation, 2) node selection and signal extraction, 3) BFN construction, and 4) classification with feature selection.

Table 1. Demographic and clinical information of subjects in the ADNI and ABIDE datasets.

Datasets	Category	Gender (Male/Female)	Age (Mean ± SD)
ABIDE	ASD (N = 79)	68/11	14.51 ± 6.23
	HC (N = 105)	79/26	15.80 ± 3.23
ADNI	MCI (N = 68)	39/29	72.82 ± 7.66
	HC (N = 69)	17/52	75.29 ± 5.34

ADNI database: 137 subjects (68 MCIs and 69 HCs) are utilized in this study, in which all participants were scanned by 3.0 T Philip scanners. The scanning parameters are as follows: TE is 3000 ms, TR is 300 ms, voxel thickness is 3.3 mm, and imaging matrix is 64 × 64. For each subject, the scanning time was 7 min, corresponding to 140 volumes.

The acquired rs-fMRI data on two benchmark databases were preprocessed with SPM8 toolbox3 and DPABI [20]. Specifically, the first 5 rs-fMRI volumes of each voxel were discarded. The remaining volumes are processed as follows: 1) slice timing for the remaining volumes and correcting head motion correction (*i.e.*, subjects with head motion larger than 2 mm or 2° were excluded); 2) regressing out the nuisance signals (ventricle, white matter, and head-motion) based on the Friston 24-parameter model [21]; 3) registering the corrected rs-fMRI images to Montreal Neurological Institute (MNI) standard space [22]; 4) spatially smoothing the images by a kernel of 6 mm; 5) temporal filtering (0.01 - 0.10 Hz). Finally, according to the automated anatomical labeling (AAL) atlas [23], the brain was divided into 116 ROIs.

2.2. Baseline Methods for BFN Construction

Once the representative time series has been extracted by averaging all the voxel signals within the current ROI, the next step is to calculate the connectivity between every possible pair of ROIs. To estimate BFN, several common approaches have been proposed in the past decades, such as PC, partial correlation [24],

Granger causality [25], Bayesian network [26], Patel's conditional dependence [27].

PC, as the most popular and simplest approach for constructing BFNs [19], which is used in this paper as a basic method for constructing BFNs, can be defined as follows mathematically:

$$w_{ij} = \frac{\left(x_i - \overline{x}_i\right)^{\mathrm{T}}\left(x_j - \overline{x}_j\right)}{\sqrt{\left(x_i - \overline{x}_i\right)^{\mathrm{T}}\left(x_i - \overline{x}_i\right)}\sqrt{\left(x_j - \overline{x}_j\right)^{\mathrm{T}}\left(x_j - \overline{x}_j\right)}} \tag{1}$$

where $x_i \in R^t, i \in 1,\cdots,d$ is the mean time series extracted from i-th brain region, t is the number of time points in each series, d is the total number of ROIs, $\overline{x}_i \in R^t$ is the mean of x_i, and $w_{ij}, i, j \in 1,\cdots,d$ is the connection weight between i-th ROI and j-th ROI. Without loss of generality, we redefine. That is, the new x_i has been centralized by $x_i - \overline{x}_i$ and normalized by $\sqrt{\left(x_i - \overline{x}_i\right)^{\mathrm{T}}\left(x_i - \overline{x}_i\right)}$.

Thus, we can simplify Equation (1) and have $w_{ij} = x_i^{\mathrm{T}} x_j$. Equivalently, we can obtain the adjacency matrix of BFN via solving the following regression model,

$$\min_{w_{ij}} \sum_{ij}^{n} \left\| x_i - w_{ij} x_j \right\|^2 \tag{2}$$

According to a previous work [28], Equation (2) can be further transformed mathematically into the following matrix form:

$$\min_{W} \left\| W - X^{\mathrm{T}} X \right\|_F^2 \tag{3}$$

where $W = \left(w_{ij}\right) \in R^{d\times d}$ is the correlation matrix of the estimated BFN, $X = \left[x_1, x_2, \cdots, x_d\right] \in R^{d\times d}$ is the data matrix, and $\|.\|_F$ represents the Frobenius-norm of a matrix.

2.3. The Proposed Method for BFN Construction

According to the AAL template, the brain is divided into 116 ROIs with varying numbers of voxels (for example, the largest ROI contains 1512 voxels, while the smallest one contains only 11 voxels). To facilitate comparison, we uniformly extract n (We empirically set n = 11 in this work.) nodes in each brain region. As mentioned earlier, K-means and PCA are used by us to extract nodes of each ROI. Kmeans method is to distinguish a ROI into uniform n nodes according to the three-dimensional spatial position coordinates of voxels, and then averages the BOLD signals of all voxels in each node as the representative signal of this node. And PCA method is to use the voxel signals in current ROI as a matrix, and the n eigenvectors corresponding to its first n maximum eigenvalues are the time series of n nodes. Next, CCA, as a multivariate statistical method that goes beyond techniques that map one-to-one relations (e.g., PC) or manyto-one relations (e.g., ordinary multiple regression) [18], is used by us to calculate the relationship between time series corresponding to two sets of nodes from two ROIs. In what follows, we present the model and algorithm of CCA in detail.

1) Models: CCA can be described by the following optimization model:

$$\left(w_i, w_j\right) = \arg\min_{w_i, w_j} \frac{w_i^{\mathrm{T}} X_i^{\mathrm{T}} X_j w_j}{\sqrt{w_i^{\mathrm{T}} X_i^{\mathrm{T}} X_i w_i \bullet w_j^{\mathrm{T}} X_j^{\mathrm{T}} X w_j}} \tag{4}$$

where $X_i = \left[x_1^i, x_2^i, \cdots, x_m^i, \cdots, x_p^i\right] \in R^{t\times p}$ is the time series of the i-th ROI, and $x_m^i \in R^{t\times 1}$ is the time series of the m-th voxel in the i-th ROI. $w_i \in R^{p\times 1}$ is the weight vector whose dimension p is determined by the number of voxels in the i-th ROI. Equally, Equation (4) can be rewritten by the following matrix form in mathematic:

$$\begin{aligned} &\max_{w_i, w_j} w_i^{\mathrm{T}} X_i^{\mathrm{T}} X_j w_j \\ &\text{s.t. } w_i^{\mathrm{T}} X_i^{\mathrm{T}} X^{\mathrm{T}} w_i = 1 \\ &\quad w_j^{\mathrm{T}} X_j^{\mathrm{T}} X_j w_j = 1 \end{aligned} \tag{5}$$

2) Algorithms: Accordingly, Equation (5) can be transformed to the following formula by Lagrange multiplier method:

$$L\left(w_i, w_j\right) = w_i^{\mathrm{T}} X_i^{\mathrm{T}} X_j w_j - \frac{\lambda_1}{2}\left(w_i^{\mathrm{T}} X_i^{\mathrm{T}} X_i w_i - 1\right) - \frac{\lambda_2}{2}\left(w_j^{\mathrm{T}} X_j^{\mathrm{T}} X_j w_j - 1\right) \tag{6}$$

λ_1 and λ_2 in Equation (6) are Lagrange multipliers, and The next step is to find the partial derivatives for w_i and w_j, respectively.

$$\frac{\partial L}{\partial w_i} = X_i^{\mathrm{T}} X_j w_j - \lambda_1 X_i^{\mathrm{T}} X_i w_i = 0 \tag{7}$$

$$\frac{\partial L}{\partial w_j} = X_j^{\mathrm{T}} X_i w_i - \lambda_2 X_j^{\mathrm{T}} X_j w_j = 0 \tag{8}$$

To address this kind of optimization problem, multiply Equation (7) by w_i^{T} and Equation (8) by w_j^{T}, respectively

$$w_i^{\mathrm{T}} X_i^{\mathrm{T}} X_j w_j = \lambda_1 w_i^{\mathrm{T}} X_i^{\mathrm{T}} X_i w_i = \lambda_1 \tag{9}$$

$$w_j^{\mathrm{T}} X_j^{\mathrm{T}} X_i w_i = \lambda_2 w_j^{\mathrm{T}} X_j^{\mathrm{T}} X_j w_j = \lambda_2 \tag{10}$$

So from Equation (9) and Equation (10) we get that

$$\lambda_1 = \lambda_1^{\mathrm{T}} = \left(w_i^{\mathrm{T}} X_i^{\mathrm{T}} X_j w_j\right)^{\mathrm{T}} = w_j^{\mathrm{T}} X_j^{\mathrm{T}} X_i w_i = \lambda_2 \tag{11}$$

Let $\lambda_1 = \lambda_2 = \lambda$, Equation (7) and Equation (8) can be rewritten as

$$X_i^{\mathrm{T}} X_j w_j - \lambda X_i^{\mathrm{T}} X_i w_i = 0 \tag{12}$$

$$X_j^{\mathrm{T}} X_i w_i - \lambda X_j^{\mathrm{T}} X_j w_j = 0 \tag{13}$$

Equivalently, it can be further simplified to the following form:

$$X_i^{\mathrm{T}} X_j \left(X_j^{\mathrm{T}} X_j\right)^{-1} X_j^{\mathrm{T}} X_i w_i = \lambda^2 X_i^{\mathrm{T}} X_i w_i \tag{14}$$

$$X_j^{\mathrm{T}} X_i \left(X_i^{\mathrm{T}} X_i\right)^{-1} X_i^{\mathrm{T}} X_j w_j = \lambda^2 X_j^{\mathrm{T}} X_j w_j \tag{15}$$

The optimization problem is equivalent to the following eigenvalue problem:

$$\begin{pmatrix} & X_i^{\mathrm{T}} X_j \\ X_j^{\mathrm{T}} X_i & \end{pmatrix} \begin{pmatrix} w_i \\ w_j \end{pmatrix} = \lambda \begin{pmatrix} X_i^{\mathrm{T}} X_i & \\ & X_j^{\mathrm{T}} X_j \end{pmatrix} \begin{pmatrix} w_i \\ w_j \end{pmatrix} \tag{16}$$

3. Experiments and Results

In this section, we introduce the primary experimental procedure, the experimental setup and the classification results for different methods.

3.1. Experimental Setup

After obtaining the FBNs of all subjects, the subsequent task comes to use the constructed BFNs to train a classifier for identifying ASDs from HCs. In our experiment, we use the network edge weights as features for ASD identification. As described above, the preprocessed data is parceled into 116 brain regions, and so we have a high feature dimension of $116\times(116-1)/2=6670$ from the symmetric BFN adjacent matrix. Since the BFN matrix is symmetric, we just use its upper triangular elements as input features for classification. Even so, it still causes the curse of dimensionality [29], since the number of feature dimension is far greater than the sample size (*i.e.*, the number of subjects used in our experiment). To address this problem, numbers of approaches for feature selection have been proposed such as t-test, least absolute shrinkage and selection operator (LASSO) [30], genetic algorithm (GA) [31], and so on. In this paper, we apply the simplest t-test with two accepted *p*-values (0.01 and 0.05) for feature selection and choose the linear support vector machine (SVM) classifier (C = 1) to conduct the subsequent classification task. The final classification accuracy of involved methods is evaluated by 100 validation (5-fold CV).

3.2. Classification Results

To evaluate the different BFN estimation methods, five evaluation metrics are utilized in this experiment, including accuracy (ACC), specificity (SPE), sensitivity (SEN), F1-score (F1) and AUC (the area under the receiver operating characteristic (ROC) curve). Specifically, the mathematical definition of these three metrics is given as follows:

$$\mathrm{ACC} = \frac{\mathrm{TP}+\mathrm{TN}}{\mathrm{TP}+\mathrm{FP}+\mathrm{TN}+\mathrm{FN}}, \tag{17}$$

$$\mathrm{SEN} = \frac{\mathrm{TP}}{\mathrm{TP}+\mathrm{FN}}, \tag{18}$$

$$\mathrm{SPE} = \frac{\mathrm{TN}}{\mathrm{FP}+\mathrm{TN}}, \tag{19}$$

$$\mathrm{F}_1 = \frac{2\mathrm{TP}}{2\mathrm{TP}+\mathrm{FN}+\mathrm{FP}}, \tag{20}$$

where TP, TN, FP and FN represent true positive, true negative, false positive and false negative respectively.

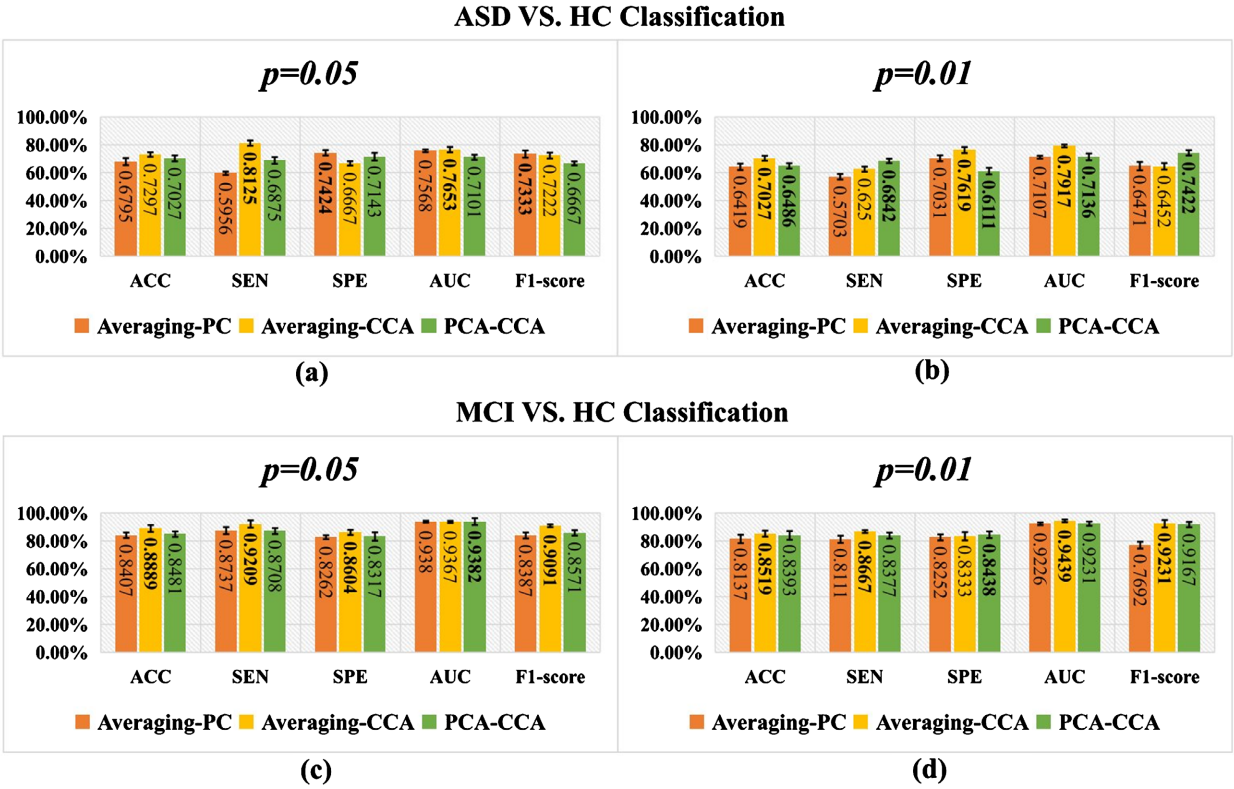

Figure 3. The classification results (mean ± standard deviation) base on five performance metrics (*i.e.*, ACC, SEN, SPE, AUC and F1) by three different methods (*i.e.*, Averaging-PC, Averaging-CCA and PCA-CCA methods) for ASD/MCI identification. Where the best results for each set of metrics are represented by bold numbers.

Results of ASD Identification:

As can be seen from Figure 3(c), Figure 3(d) and Figure 4(c), Figure 4(d), the proposed method is superior to the baseline method under five evaluation metrics (*i.e.*, ACC, SEN, SPE, AUC and F_1). Especially for AveragingCCA method, it achieves the best performance on ACC, SEN and F_1. Therefore, we argue that the method proposed in this paper may have practical significance for the timely diagnosis of MCI population.

4. Discussion

In this section, we first discuss the effect of the number of nodes in each brain region in ASD/MCI classification. Then, we investigate the effect of brain parcellation on the classification results. Finally, we show the most discriminative features selected by proposed methods for exploring their relationship with brain disorders.

4.1. Influence of Number of Node

Due to the complexity and unknown nature of BFNs, the optimal value n of the number of nodes is a practical problem that we need to consider. As we mentioned in Section II-C, the smallest ROI defined by AAL atlas contains only 11 voxels. Thus, to keep the number of voxels within ROIs, the number of nodes n

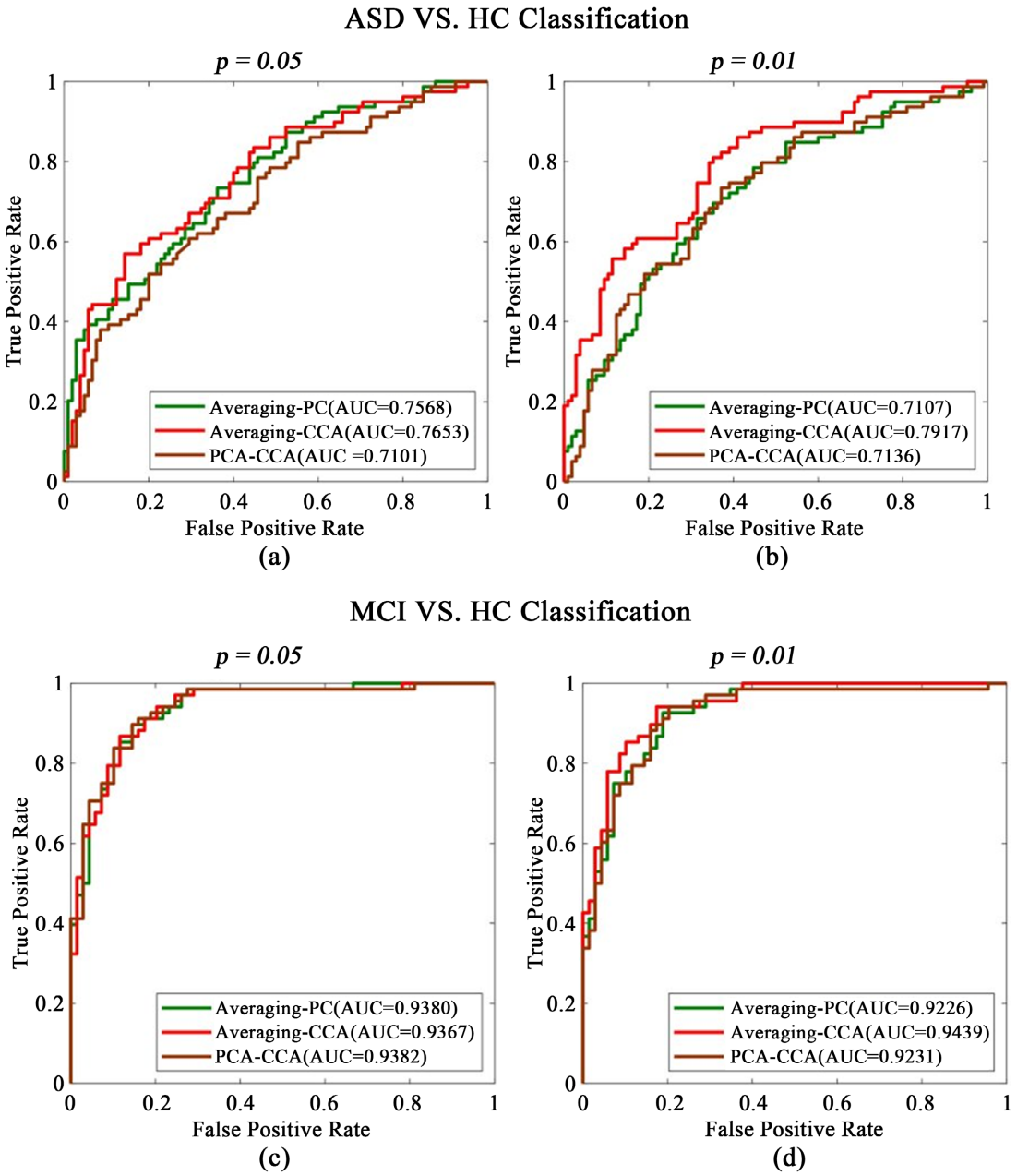

Figure 4. The ROC curves and AUC values achieved by three different methods under two accepted *p*-values (*i.e.*, 0.05, 0.01) in ASD/MCI classification tasks.

should be less than or equal to 11 (*i.e.*, n ≤ 11). In ASD and MCI classification tasks, based on 5-fold CV ($p = 0.05$), the classification accuracy of the Averaging-CCA and PCA-CCA methods with 11 different node number n is reported in Figure 5. It can be observed that Averaging-CCA and PCA-CCA in both ABIDE and ADNI databases achieve the best performance with n = 11 Therefore, we believe that BFN is of the best quality when n = 11.

4.2. Brain Parcellation

ROI selection is a difficult choice, as the optimal definition may vary for different

conditions or pathologies. Voxels within the same ROI tend to have similar structures and functions based on pre-defined atlases. Typical atlases include the Power [32] (a coordinate-based atlas consisting of 264 ROIs), the Harvard Oxford template [33] (a probabilistic atlas of anatomical structures and contains 118 ROIs) and the AAL [23] (a structural atlas with 116 ROIs defined from the anatomy of a reference subject). To verify the effect of different brain region atlases on the final result, in this section, we use the proposed methods (i.e. Averaing-CCA and PCACCA methods) by 100 times 5-fold CV (p-value = 0.05) to conduct the ASD and MCI classification tasks. It can be observed from Table 2: 1) In ASD VS. HC classification task, the AAL atlas can obtain the best classification

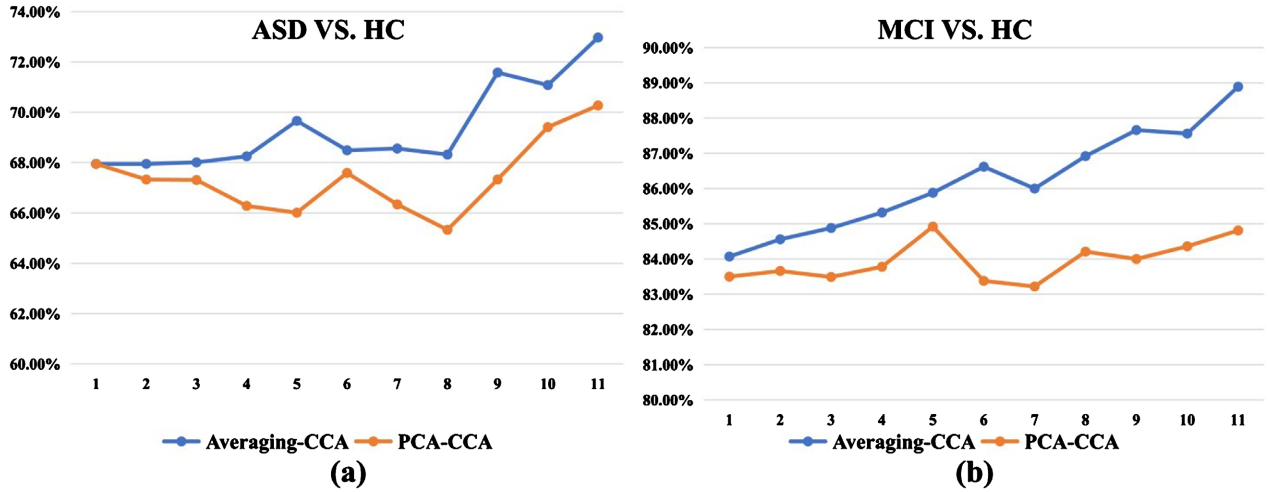

Figure 5. The classification accuracy based on Averaging-CCA and PCA-CCA methods by 11 kinds of the number of node in each ROI.

Table 2. The classification results based on the proposed methods using different atlases for brain parcellation for parcellation for ASD/MCI identification.

Datasets	Method	Atlas	ACC (%)	SEN (%)	SPE (%)	AUC (%)	F_1 (%)
ABIDE	Averaging-CCA	Power (264)	67.57	73.33	63.64	74.67	64.71
		Harard Oxford (118)	70.27	60.00	77.27	73.56	62.07
		AAL (116)	72.97	81.25	66.67	76.53	72.22
	PCA-CCA	Power (264)	70.27	66.67	72.73	73.76	64.52
		Harard Oxford (118)	64.86	58.82	70.00	72.24	60.61
		AAL (116)	70.27	68.75	71.43	71.07	66.67
ADNI	Averaging-CCA	Power (264)	85.19	82.35	90.00	92.54	87.50
		Harard Oxford (118)	85.19	85.71	84.62	94.39	85.71
		AAL (116)	88.89	92.09	86.04	93.67	90.91
	PCA-CCA	Power (264)	81.49	86.67	75.00	93.44	83.87
		Harard Oxford (118)	85.19	92.86	76.92	92.80	86.67
		AAL (116)	84.81	87.08	83.17	93.82	85.71

results when using the Averaging-CCA method, but the classification results obtained in Power atlas and AAL atlas are similar when using the PCA-CCA method. 2) In MCI VS. HC classification task, the AAL atlas can obtain relatively good results when using the Averaging-CCA method, and the results of Harvard Oxford atlas are better when using the PCA-CCA method. According to these results, we found that the performance of each atlas may vary under different conditions, so there is no best way to segment the brain. In this article, we chose the AAL atlas to predefine ROIs, mainly because of its popularity and simplicity.

4.3. Discriminative Features

In this section, to verify which features (*i.e.*, functional connections) contribute more to accuracy, we use the estimated BFN edge weights as features for classification. Based on the proposed Averaging-CCA and PCA-CCA methods, we use t-test (p-value = 0.0001) to select the most discriminating features to identify ASD and MCI populations, and show the results in Figure 6. Specially, the

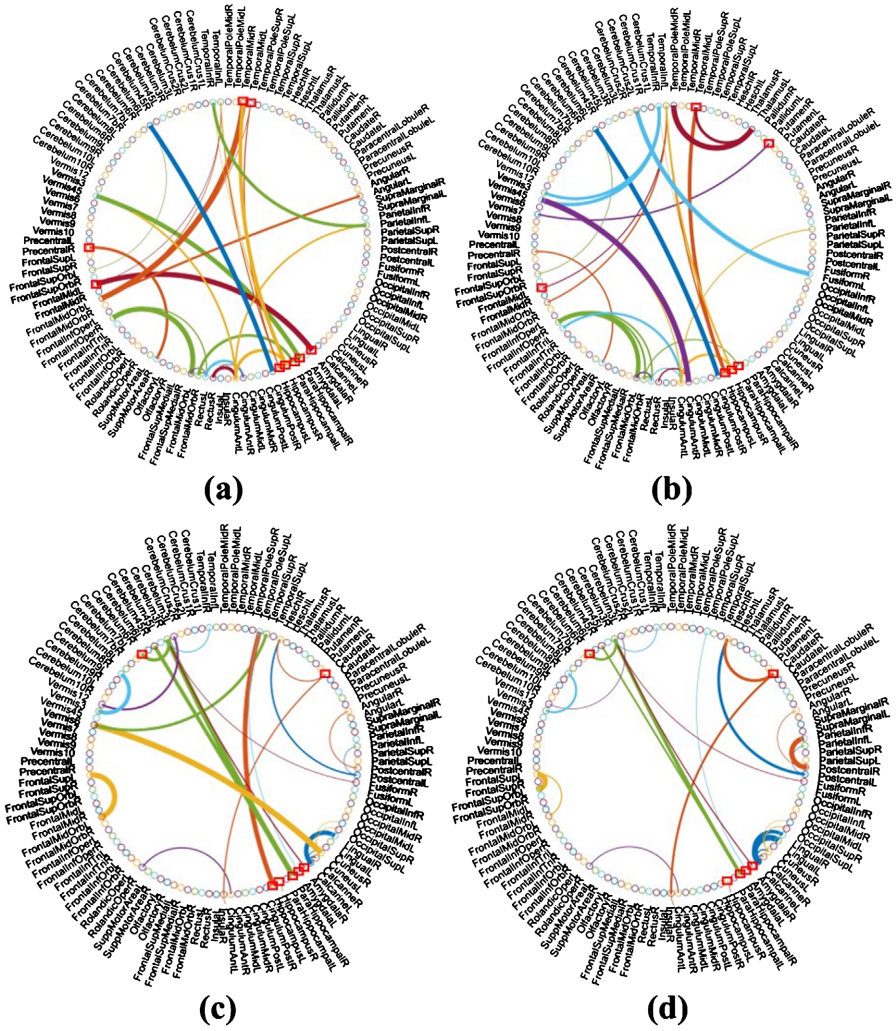

Figure 6. Most discriminative functional connections estimated by Averaging-CCA. The nodes marked by red boxes are the most discriminative ROIs for MCI/ASD identification.

thickness of each arc shown in **Figure 6** represents the discriminating ability inversely proportional to the corresponding p-value (rather than its actual connectivity strength), and for better visualization, the color of each arc is randomly assigned. In addition, we mark the selected brain regions with red boxes. For ASD identification, 28 discriminating features were selected by two methods. As shown in **Figure 6(a)**, the most important identifying features and their corresponding brain regions selected by the Averaging-CCA method include the right precentral gyrus, left middle frontal gyrus, bilateral hippocampus, bilateral parahippocampal gyrus, right amygdala and bilateral middle temporal. And the left parahippocampal gyrus, left middle frontal gyrus, right putamen, left middle temporal gyrus and bilateral hippocampus are chosen by the PCA-CCA method in **Figure 6(b)**. Many of these have been widely reported in previous studies [34] [35] [36] [37] as potential biomarkers for ASD VS. HC classification task. For MCI identification task, the Averaging-CCA and PCACCA methods selected 26 identification features respectively. It can be seen from **Figure 6(c)**, the averaging-CCA method selects brain regions that may help identify MCI include the righ parahippocampal gyrus, bilateral hippocampus, right cerebelum 6, bilateral amygdala and right caudate. And right hippocampus, right parahippocampal gyrus, right caudate, right cerebelum6 and bilateral amygdala are selected in PCACCA method in **Figure 6(d)** These regions are thought to play an important role in the default mode network and are closely related to AD or MCI, which is consistent with several previous studies [38] [39] [40] [41]. The results further prove the effectiveness of the proposed methods.

5. Conclusion

In this paper, the ROI-wise node representation method is used as a baseline method to construct BFNs. However, treating a ROI as a single node is not enough to represent the complete information about the ROI. This paper proposes a new method for obtaining nodes of ROIs based on the hypothesis that a ROI can be represented by multiple nodes, that is, to extract the node signals of ROIs with K-means or PCA, and then use CCA to construct BFNs. To investigate the validity of the proposed methods, we performed ASD vs. HC and MCI vs. HC classification tasks on two benchmark datasets with rs-fMRI data. CCA-based methods achieve high recognition rates in both ASD and MCI classification tasks. Especially, the Averaging-CCA method achieved the highest classification effect. Experimental results show that our method has a better classification effect than the baseline method, which indicates that the multiple node representation of ROIs may play an important role in mining the functional connectivity patterns of our brains. In the future, we will propose more novel BFN estimation methods for practical problems.

Acknowledgements

This work was partly supported by National Natural Science Foundation of

China (Nos. 61976110) and Natural Science Foundation of Shandong Province (Nos. ZR2018MF020).

Conflicts of Interest

The authors declare no conflicts of interest regarding the publication of this paper.

References

[1] Fox, M.D. and Raichle, M.E. (2007) Spontaneous Fluctuations in Brain Activity Observed with Functional Magnetic Resonance Imaging. *Nature Reviews Neuroscience*, **8**, 700-711. https://doi.org/10.1038/nrn2201

[2] Satterthwaite, T.D., Xia, C.H. and Bassett, D.S. (2018) Personalized Neuroscience: Common and Individual-Specific Features in Functional Brain Networks. *Neuron*, **98**, 243-245. https://doi.org/10.1016/j.neuron.2018.04.007

[3] Baio, J., Wiggins, L., Christensen, D.L., *et al.* (2018) Prevalence of Autism Spectrum Disorder among Children Aged 8 Years—Autism and Developmental Disabilities Monitoring Network, 11 Sites, United States, 2014. *MMWR Surveillance Summaries*, **67**, 1-23. https://doi.org/10.15585/mmwr.ss6706a1

[4] Mitsuru, K., Yuko, Y., Hirotoshi, H., *et al.* (2015) Reduced Long-Range Functional Connectivity in Young Children with Autism Spectrum Disorder. *Social Cognitive and Affective Neuroscience*, **10**, 248-254. https://doi.org/10.1093/scan/nsu049

[5] Selkoe, D.J. (2001) Alzheimer's Disease: Genes, Proteins, and Therapy. *Physiological Reviews*, **81**, 741-766. https://doi.org/10.1152/physrev.2001.81.2.741

[6] Mckhann, G. (1984) Clinical Diagnosis of Alzheimer's Disease: Report of the NINCDS-ADRDA Work Group under the Auspices of Department of Health and Human Services Task Force on Alzheimer's Disease. *Neurology*, **34**, Article No. 939. https://doi.org/10.1212/WNL.34.7.939

[7] Reijneveld, J.C., Ponten, S.C., Berendse, H.W. and Stam, C.J. (2007) The Application of Graph Theoretical Analysis to Complex Networks in the Brain. *Clinical Neurophysiology*, **118**, 2317-2331. https://doi.org/10.1016/j.clinph.2007.08.010

[8] De Reus, M.A. and Van den Heuvel, M.P. (2013) The Parcellation-Based Connectome: Limitations and Extensions. *NeuroImage*, **80**, 397-404. https://doi.org/10.1016/j.neuroimage.2013.03.053

[9] Wiener, M., Turkeltaub, P. and Coslett, H.B. (2009) The Image of Time: A Voxel-Wise Meta-Analysis. *NeuroImage*, **49**, 1728-1740. https://doi.org/10.1016/j.neuroimage.2009.09.064

[10] Beckmann, C. (2012) Modelling with Independent Components. *NeuroImage*, **62**, 891-901. https://doi.org/10.1016/j.neuroimage.2012.02.020

[11] Cole, D.M., Smith, S.M. and Beckmann, C.F. (2010) Advances and Pitfalls in the Analysis and Interpretation of Resting-State FMRI Data. *Frontiers in Systems Neuroscience*, **4**, Article No. 8. https://doi.org/10.3389/fnsys.2010.00008

[12] Zang, Y., Jiang, T., Lu, Y., *et al.* (2004) Regional Homogeneity Approach to fMRI Data Analysis. *NeuroImage*, **22**, 394-400. https://doi.org/10.1016/j.neuroimage.2003.12.030

[13] Zou, Q., Zhu, C., Yang, Y., *et al.* (2008) An Improved Approach to Detection of Amplitude of Low-Frequency Fluctuation (ALFF) for Resting-State fMRI: Fractional ALFF. *Journal of Neuroscience Methods*, **172**, 137-141.

https://doi.org/10.1016/j.jneumeth.2008.04.012

[14] Stanley, M.L., Moussa, M.N., Paolini, B.M., *et al.* (2013) Defining Nodes in Complex Brain Networks. *Frontiers in Computational Neuroscience*, **7**, Article No. 169. https://doi.org/10.3389/fncom.2013.00169

[15] David, P., Massimiliano, Z. and Buldu, J. (2014) Reconstructing Functional Brain Networks: Have We Got the Basics Right? *Frontiers in Human Neuroscience*, **8**, Article No. 107. https://doi.org/10.3389/fnhum.2014.00107

[16] Kanungo, T., Mount, D.M., Netanyahu, N.S., *et al.* (2002) An Efficient k-Means Clustering Algorithm: Analysis and Implementation. *IEEE Transactions on Pattern Analysis and Machine Intelligence*, **24**, 881-892. https://doi.org/10.1109/TPAMI.2002.1017616

[17] Yeung, K.Y. and Ruzzo, W.L. (2019) Principal Component Analysis for Clustering Gene Expression Data. *Bioinformatics* (*Oxford*, *England*), **17**, 763-774. https://doi.org/10.1093/bioinformatics/17.9.763

[18] Wang, H.T., Smallwood, J., Mourao-Miranda, J., Xia, C.H. and Bzdok, D. (2020) Finding the Needle in a High-Dimensional Haystack: Canonical Correlation Analysis for Neuroscientists. *NeuroImage*, **216**, Article ID: 116745. https://doi.org/10.1016/j.neuroimage.2020.116745

[19] Smith, S.M., Vidaurre, D., Beckmann, C.F., *et al.* (2013) Functional Connectomics from Resting-State fMRI. *Trends in Cognitive Sciences*, **17**, 666-682. https://doi.org/10.1016/j.tics.2013.09.016

[20] Yan, C. and Zang, Y. (2010) DPARSF: A MATLAB Toolbox for "Pipeline" Data Analysis of Resting-State fMRI. *Frontiers in Systems Neuroscience*, **4**, Article No. 13. https://doi.org/10.3389/fnsys.2010.00013

[21] Friston, K.J., Williams, S., Howard, R., Frackowiak, R.S. and Turner, R. (1996) Movement-Related Effects in fMRI Time-Series. *Magnetic Resonance in Medicine*, **35**, 346-355. https://doi.org/10.1002/mrm.1910350312

[22] Brett, M., Christoff, K., Cusack, R. and Lancaster, J.L. (2001) Using the Talairach Atlas with the MNI Template. *NeuroImage*, **13**, Article No. 85. https://doi.org/10.1016/S1053-8119(01)91428-4

[23] Tzourio-Mazoyer, N., Landeau, B., Papathanassiou, D., *et al.* (2002) Automated Anatomical Labeling of Activations in SPM Using a Macroscopic Anatomical Parcellation of the MNI MRI Single-Subject Brain. *NeuroImage*, **15**, 273-289. https://doi.org/10.1006/nimg.2001.0978

[24] Radok, U. and Brown, T.J. (2009) Anomaly Correlation and an Alternative: Partial Correlation. *Monthly Weather Review*, **121**, 1269-1271. https://doi.org/10.1175/1520-0493(1993)121<1269:ACAAAP>2.0.CO;2

[25] Roebroeck, A., Formisano, E. and Goebel, R. (2005) Mapping Directed Influence over the Bra Using Granger Causality and fMRI. *NeuroImage*, **25**, 230-242. https://doi.org/10.1016/j.neuroimage.2004.11.017

[26] Ide, J.S., Sheng, Z. and Li, C. (2014) Bayesian Network Models in Brain Functional Connectivity Analysis. *International Journal of Approximate Reasoning*, **56**, 23-35. https://doi.org/10.1016/j.ijar.2013.03.013

[27] Dawson, D.A., Cha, K., Lewis, L.B., Mendola, J.D. and Shmuel, A. (2013) Evaluation and Calibration of Functional Network Modeling Methods Based on Known Anatomical Connections. *NeuroImage*, **67**, 331-343. https://doi.org/10.1016/j.neuroimage.2012.11.006

[28] Jiang, X., Zhang, L., Qiao, L. and Shen, D. (2019) Estimating Functional Connectiv-

ity Networks via Low-Rank Tensor Approximation with Applications to MCI Identification. *IEEE Transactions on Biomedical Engineering*, **67**, 1912-1920. https://doi.org/10.1109/TBME.2019.2950712

[29] Hinton, G.E. and Salakhutdinov, R.R. (2006) Reducing the Dimensionality of Data with Neural Networks. *Science*, **313**, 504-507. https://doi.org/10.1126/science.1127647

[30] Tibshirani, R. (1996) Regression Shrinkage and Selection via the LASSO. *Journal of the Royal Statistical Society*: *Series B* (*Methodological*), **58**, 267-288. https://doi.org/10.1111/j.2517-6161.1996.tb02080.x

[31] Szenkovits, A., Meszlenyi, R., Buza, K., Gasko, N., Lung, R.I. and Suciu, M. (2018) Feature Selection with a Genetic Algorithm for Classification of Brain Imaging Data. In: Stańczyk, U., Zielosko, B. and Jain, L.C., Eds., *Advances in Feature Selection for Data and Pattern Recognition*, Springer, Berlin, 185-202. https://doi.org/10.1007/978-3-319-67588-6_10

[32] Power, J.D., Cohen, A.L., Nelson, S.M., *et al.* (2011) Functional Network Organization of the Human Brain. *Neuron*, **72**, 665-678. https://doi.org/10.1016/j.neuron.2011.09.006

[33] Desikan, R.S., Segonne, F., Fischl, B., *et al.* (2006) An Automated Labeling System for Subdividing the Human Cerebral Cortex on MRI Scans into Gyral Based Regions of Interest. *NeuroImage*, **31**, 968-980. https://doi.org/10.1016/j.neuroimage.2006.01.021

[34] Ecker, C., Bookheimer, S.Y. and Murphy, D. (2015) Neuroimaging in Autism Spectrum Disorder: Brain Structure and Function across the Lifespan. *The Lancet Neurology*, **14**, 1121-1134. https://doi.org/10.1016/S1474-4422(15)00050-2

[35] Toal, F., Bloemen, O.J.N., Deeley, Q., *et al.* (2009) Psychosis and Autism: Magnetic Resonance Imaging Study of Brain Anatomy. *The British Journal of Psychiatry*, **102**, 418-425. https://doi.org/10.1192/bjp.bp.107.049007

[36] Ecker, C., Rocha-Rego, V., Johnston, P., *et al.* (2010) Investigating the Predictive Value of Whole-Brain Structural MR Scans in Autism: A Pattern Classification Approach. *NeuroImage*, **49**, 44-56. https://doi.org/10.1016/j.neuroimage.2009.08.024

[37] Sparks, B.F., Friedman, S., Shaw, D.W.W., *et al.* (2002) Brain Structural Abnormalities in Young Children with Autism Spectrum Disorder. *Neurology*, **59**, 184-192. https://doi.org/10.1212/WNL.59.2.184

[38] Xu, L., Wu, X., Li, R., *et al.* (2016) Prediction of Progressive Mild Cognitive Impairment by Multi-Modal Neuroimaging Biomarkers. *Journal of Alzheimer's Disease*, **51**, 1045-1056. https://doi.org/10.3233/JAD-151010

[39] Yu, R., Zhang, H., An, L., *et al.* (2017) Connectivity Strength-Weighted Sparse Group Representation-Based Brain Network Construction for MCI Classification. *Human Brain Mapping*, **38**, 2370-2383. https://doi.org/10.1002/hbm.23524

[40] Zhu, X., Suk, H.-I., Lee, S.-W. and Shen, D. (2016) Subspace Regularized Sparse Multitask Learning for Multiclass Neurodegenerative Disease Identification. *IEEE Transactions on Biomedical Engineering*, **63**, 607-618. https://doi.org/10.1109/TBME.2015.2466616

[41] He, Y., Wang, L., Zang, Y., *et al.* (2007) Regional Coherence Changes in the Early Stages of Alzheimer's Disease: A Combined Structural and Resting-State Functional MRI Study. *NeuroImage*, **35**, 488-500. https://doi.org/10.1016/j.neuroimage.2006.11.042